2002

Three-dimensional Landau theory for multivariant stress-induced martensitic phase transformations. II.   Multivariant phase transformations and stress space analysis

Valery I. Levitas, *Texas Tech University*
Dean L. Preston, *Los Alamos National Laboratory*

Three-dimensional Landau theory for multivariant stress-induced martensitic phase transformations.
II.   Multivariant phase transformations and stress space analysis

Valery I. Levitas[1,*] and Dean L. Preston[2]

[1]*Texas Tech University, Department of Mechanical Engineering, Lubbock, Texas 79409-1021*
[2]*Applied Physics Division, Los Alamos National Laboratory, Los Alamos, New Mexico 87545*

In this paper, the three-dimensional Landau model of austenite-martensite transformations constructed in Part I is generalized to include transformations between an arbitrary number of martensitic variants. The model can incorporate all temperature-dependent thermomechanical properties of both phases for arbitrary crystal symmetries, including higher-order elastic constants, and it correctly describes the characteristic features of stress-strain curves for shape-memory alloys and steels, namely, constant transformation strain tensors, constant or weakly temperature dependent stress hysteresis, and transformation at nonzero tangent moduli. Geometric representations of the conditions for phase equilibrium and phase transformations in six-dimensional stress space are developed. For the cubic-tetragonal phase transformation, equilibrium and transformation surfaces in three-dimensional stress space and the corresponding lines in the deviatoric-stress plane are found at various temperatures, and transformation processes are analyzed. All model parameters are obtained for the NiAl cubic-tetragonal phase transformation using the results of molecular dynamics simulations available in the literature.

I. INTRODUCTION

This paper is organized as follows. In Sec. II, the framework developed in part I for the description of phase transformations (PT's) between austenite A and martensite M is applied to transformations between two martensitic variants. Equations obtained contain material parameters which do not appear in the description of the $A \leftrightarrow M$ PT.

In Sec. III we formulate and solve the problem of constructing a Gibbs potential that describes both austenite-martensite transformations and transformations between an arbitrary number of martensitic variants M_i. To make the theory consistent with results obtained in part I for the $A \leftrightarrow M$ PT and for variant-variant PT, we employ a 2-3-4-5 polynomial in the order parameter η_i. Variations in the topography of the free energy surface due to changes in temperature and stress are analyzed in detail for a two-dimensional cubic-tetragonal system. Section IV is a brief discussion of the symmetries of our Gibbs potential.

In Sec. V, geometric representations of the conditions for phase equilibrium and phase transformations in six-dimensional stress space are developed and studied. This construction dramatically simplifies the analysis of multivariant transformations for general stress states. For the cubic to tetragonal PT, equilibrium and transformation surfaces in three-dimensional stress space and the corresponding lines in the deviatoric-stress plane are found at various temperatures, and the corresponding transformation processes are analyzed in some detail. The validity of the associated transformation rule, the corresponding extremum principle, and the nonconcavity of the regions of stability and metastability of A and all M_i are demonstrated.

In Sec. VI, all model parameters for the NiAl cubic-tetragonal PT are obtained using published molecular dynamics data. Phase equilibrium and transformation conditions are analyzed. Our concluding remarks are made in Sec. VII.

II. TRANSFORMATIONS BETWEEN TWO MARTENSITIC VARIANTS

The transformation $M_1 \rightarrow M_2$ from M_1 with transformation strain $\boldsymbol{\varepsilon}_{t1}$ to M_2 with transformation strain $\boldsymbol{\varepsilon}_{t2}$ is called a reorientation process. It can be described with the Gibbs potential we derived for the $A \leftrightarrow M$ PT[1] but slightly modified to account for nonzero transformation strain in the initial state and equal thermal parts of the Gibbs free energies for both phases:

$$G(\boldsymbol{\sigma}, \theta, \eta) = -\boldsymbol{\sigma}{:}\boldsymbol{\lambda}{:}\boldsymbol{\sigma}/2 - \boldsymbol{\sigma}{:}\boldsymbol{\varepsilon}_t(\eta) + \bar{A}\,\eta^2(1-\eta)^2, \quad (1)$$

$$\boldsymbol{\varepsilon}_t(\eta) = \boldsymbol{\varepsilon}_{t1} + (\boldsymbol{\varepsilon}_{t2} - \boldsymbol{\varepsilon}_{t1})[\bar{a}\,\eta^2 + (4 - 2\bar{a})\,\eta^3 + (\bar{a} - 3)\,\eta^4]. \quad (2)$$

Here $\boldsymbol{\sigma}$ is the stress tensor, $\boldsymbol{\lambda}$ is the second-order fourth-rank elastic compliance tensor, $\bar{A}$ and $\bar{a}$ are material parameters, and η is the order parameter which varies from 0 for M_1 to 1 for M_2. The difference between the Gibbs potentials of the martensitic variants, which is the macroscopic driving force for the $M_1 \rightarrow M_2$ transformation, is

$$G(\boldsymbol{\sigma}, \theta, 0) - G(\boldsymbol{\sigma}, \theta, 1) = \boldsymbol{\sigma}{:}(\boldsymbol{\varepsilon}_{t2} - \boldsymbol{\varepsilon}_{t1}). \quad (3)$$

Conditions for $M_1 \rightarrow M_2$ and $M_2 \rightarrow M_1$ can be obtained from the corresponding equations in Ref. 1 for $A \rightarrow M$ and $M \rightarrow A$ by substituting $\boldsymbol{\varepsilon}_{t2} - \boldsymbol{\varepsilon}_{t1}$ for $\boldsymbol{\varepsilon}_t$, $\bar{A}$ for A, $\bar{a}$ for a, and $\Delta G^\theta = 0$. In particular, from Eq. (14) in Ref. 1

$$A \to M: \quad \boldsymbol{\sigma}{:}\boldsymbol{\varepsilon}_t \geq \frac{A}{a}, \quad M \to A: \quad \boldsymbol{\sigma}{:}\boldsymbol{\varepsilon}_t \leq \frac{6\Delta G^\theta - A}{6-a} \quad (4)$$

one obtains

$$M_1 \to M_2: \quad \boldsymbol{\sigma}{:}(\boldsymbol{\varepsilon}_{t2} - \boldsymbol{\varepsilon}_{t1}) \geq \frac{\bar{A}}{\bar{a}},$$

$$M_2 \to M_1: \quad \boldsymbol{\sigma}{:}(\boldsymbol{\varepsilon}_{t2} - \boldsymbol{\varepsilon}_{t1}) \leq -\frac{\bar{A}}{6-\bar{a}}. \quad (5)$$

Since the magnitudes of the stresses for the $M_1 \to M_2$ and $M_2 \to M_1$ transformations are expected to be the same, it follows from Eq. (5) that $\bar{a} = 3$. For $\bar{a} = 3$, the condition for the loss of stability of M_1 is

$$\partial^2 G(\boldsymbol{\sigma}, \theta, 0)/\partial \eta^2 = -6\boldsymbol{\sigma}{:}(\boldsymbol{\varepsilon}_{t2} - \boldsymbol{\varepsilon}_{t1}) + 2\bar{A} \leq 0. \quad (6)$$

The condition for $M_2 \to M_1$ is obtained by evaluating the second derivative at $\eta = 1$ and interchanging indices 1 and 2.

It is straightforward to include η-dependent thermal strain and elastic compliances through fourth order

$$G = -\boldsymbol{\sigma}{:}\boldsymbol{\lambda}(\eta){:}\boldsymbol{\sigma}/2 - [\boldsymbol{\sigma}{:}\boldsymbol{\lambda}^3(\eta){:}\boldsymbol{\sigma}]{:}\boldsymbol{\sigma}/3$$
$$- \boldsymbol{\sigma}{:}[\boldsymbol{\sigma}{:}\boldsymbol{\lambda}^4(\eta){:}\boldsymbol{\sigma}]{:}\boldsymbol{\sigma}/4 - \boldsymbol{\sigma}{:}[\boldsymbol{\varepsilon}_t(\eta) + \boldsymbol{\varepsilon}_\theta(\eta)]$$
$$+ \bar{A}\eta^2(1-\eta)^2, \quad (7)$$

$$\boldsymbol{\varepsilon}_\theta(\eta) = \boldsymbol{\varepsilon}_{\theta 1} + (\boldsymbol{\varepsilon}_{\theta 2} - \boldsymbol{\varepsilon}_{\theta 1})[\bar{a}_\theta \eta^2 + (4-2\bar{a}_\theta)\eta^3 + (\bar{a}_\theta - 3)\eta^4],$$

$$\boldsymbol{\lambda}^m(\eta) = \boldsymbol{\lambda}_1^m + (\boldsymbol{\lambda}_2^m - \boldsymbol{\lambda}_1^m)[\bar{a}_{m\lambda}\eta^2$$
$$+ (4 - 2\bar{a}_{m\lambda})\eta^3 + (\bar{a}_{m\lambda} - 3)\eta^4], \quad (8)$$

where $\boldsymbol{\lambda}{:=}\boldsymbol{\lambda}^2$. Equations (8) are motivated by Eq. (2). From the condition that the magnitudes of the stresses for the $M_1 \to M_2$ and $M_2 \to M_1$ transformations be the same, one obtains $\bar{a}_\theta = \bar{a}_{m\lambda} = 3$ and

$$\boldsymbol{\varepsilon}_\theta(\eta) = \boldsymbol{\varepsilon}_{\theta 1} + (\boldsymbol{\varepsilon}_{\theta 2} - \boldsymbol{\varepsilon}_{\theta 1})\eta^2(3 - 2\eta),$$

$$\boldsymbol{\lambda}^m(\eta) = \boldsymbol{\lambda}_1^m + (\boldsymbol{\lambda}_2^m - \boldsymbol{\lambda}_1^m)\eta^2(3 - 2\eta). \quad (9)$$

The condition for the loss of stability of M_1 is

$$\partial^2 G(\boldsymbol{\sigma}, \theta, 0)/\partial \eta^2 = -6\boldsymbol{\sigma}{:}(\boldsymbol{\varepsilon}_{t2} - \boldsymbol{\varepsilon}_{t1}) - 6\boldsymbol{\sigma}{:}(\boldsymbol{\varepsilon}_{\theta 2} - \boldsymbol{\varepsilon}_{\theta 1})$$
$$- 3\boldsymbol{\sigma}{:}(\boldsymbol{\lambda}_2 - \boldsymbol{\lambda}_1){:}\boldsymbol{\sigma}$$
$$- 2[\boldsymbol{\sigma}{:}(\boldsymbol{\lambda}_2^3 - \boldsymbol{\lambda}_1^3){:}\boldsymbol{\sigma}]{:}\boldsymbol{\sigma}$$
$$- 3\boldsymbol{\sigma}{:}[\boldsymbol{\sigma}{:}(\boldsymbol{\lambda}_2^4 - \boldsymbol{\lambda}_1^4){:}\boldsymbol{\sigma}]{:}\boldsymbol{\sigma}/2 + 2\bar{A} \leq 0. \quad (10)$$

The condition for the loss of stability of M_2 is obtained from that for M_1 by just interchanging variant indices 1 and 2. The general theory, which simultaneously describes the $A \to M_i$ and $M_i \to M_j$ PT, must reduce to the equations of this section. As we will see in the next section, this is a strong constraint on the general theory.

III. MULTIVARIANT PHASE TRANSFORMATIONS

We now construct a Gibbs free energy for the general case of multivariant martensitic phase transformations. It reduces to our previous results for the $A \to M$ transformation obtained in Ref. 1, as well as our results for transformations between variants obtained in Sec. II.

The number of martensitic variants equals the ratio of the order (number of proper rotations) of P_A, the point group of A, to the order of P_M, the point group of M. For example, $n = 24/8 = 3$ for the cubic to tetragonal PT, $n = 24/6 = 4$ for the cubic to trigonal PT, $n = 24/4 = 6$ for the cubic to orthorhombic PT, and $n = 24/2 = 12$ for the cubic to monoclinic PT. The order parameter η_i, $i = 1, \ldots, n$, parametrizes the coset space P_A/P_M.

Let $\boldsymbol{\varepsilon}_{tk}$ be the transformation strain of martensitic variant M_k. We write the multivariant Gibbs potential in the form

$$G = -\boldsymbol{\sigma}{:}\boldsymbol{\lambda}{:}\boldsymbol{\sigma}/2$$
$$- \boldsymbol{\sigma}{:}\left(\sum_{k=1}^n \boldsymbol{\varepsilon}_{tk}[a\eta_k^2 + (4-2a)\eta_k^3 + (a-3)\eta_k^4]\right)$$
$$+ \sum_{k=1}^n [A\eta_k^2 + (4\Delta G^\theta - 2A)\eta_k^3 + (A - 3\Delta G^\theta)\eta_k^4]$$
$$+ F(\eta_1, \ldots, \eta_n), \quad (11)$$

where the order parameter η_k corresponds to transformation strain $\boldsymbol{\varepsilon}_{tk}$, the subscript 0 denotes austenite, and

$$F(\eta_1, \ldots, \eta_n) = \sum_{i=1}^{n-1} \sum_{j=i+1}^n F_{ij}(\eta_i, \eta_j) \quad (12)$$

is a function to be determined.

Define $\bar{0} = (0, \ldots, 0)$, $\overline{\eta_i} = (0, \ldots, 0, \eta_i, 0, \ldots, 0)$, and $\widehat{\eta_i} = (0, \ldots, 0, \eta_i = 1, 0, \ldots, 0)$. The multivariant Gibbs potential (11) with $F(\eta_1, \ldots, \eta_n) = 0$ correctly describes four aspects of martensitic PT.

(1) $\quad G(\boldsymbol{\sigma}, \theta, \bar{0}) - G(\boldsymbol{\sigma}, \theta, \widehat{\eta_i}) = \boldsymbol{\sigma}{:}\boldsymbol{\varepsilon}_{ti} - \Delta G^\theta \quad (13)$

is the thermodynamic driving force for the $A \leftrightarrow M_i$ PT.

(2) $\quad G(\boldsymbol{\sigma}, \theta, \widehat{\eta_i}) - G(\boldsymbol{\sigma}, \theta, \widehat{\eta_j}) = \boldsymbol{\sigma}{:}(\boldsymbol{\varepsilon}_{tj} - \boldsymbol{\varepsilon}_{ti}) \quad (14)$

as in Eq. (3).

(3) The conditions $\partial G/\partial \eta_k = 0$ result in the same equations with the same roots as in Eq. (12) in Ref. 1 for each η_k.

(4) Since $\partial^2 G/\partial \eta_i \partial \eta_j = 0$ at $\bar{0}$ and $\widehat{\eta_k}$ for $i \neq j$, the inequalities $\partial^2 G/\partial \eta_k^2 \leq 0$ at $\bar{0}$ and $\widehat{\eta_k}$ give for each k the condition for A and M_k loss of stability, respectively, as in Eq. (14) in Ref. 1.

However, there are two deficiencies in the description of PT for $F(\eta_1, \ldots, \eta_n) = 0$. First, the system of equations $\partial G/\partial \eta_k = 0$, $k = 1, \ldots, n$, has solutions with several or all $\eta_k = 1$, which means that the material point is simultaneously in several martensitic states. This shortcoming is easily remedied, for example, by substituting $(\Sigma_{k=1}^n \eta_k^2)^2$ for

the term $\Sigma_{k=1}^{n} \eta_k^4$ in G, but we will do so in another way. The second and more serious deficiency is that the transformations $M_i \leftrightarrow M_j$ are not properly described. For example, the $M_j \rightarrow M_i$ PT criterion $\partial^2 G(\widehat{\eta}_j)/\partial \eta_i^2 \leq 0$ reduces to $\boldsymbol{\sigma}{:}\boldsymbol{\varepsilon}_{ti} \geq A/a$, which is the condition for the $A \rightarrow M_i$ PT. Moreover, in order to describe reorientation, we must include additional material parameters that are not involved in the description of $A \leftrightarrow M_i$. Hence F does not vanish, and it must satisfy three requirements.

(1) It should not spoil any property of the potential G which is important for the description of the $A \leftrightarrow M_i$ PT.
(2) The condition for reorientation must be given by Eq. (6).
(3) It must remove the possibility that more than one η_k simultaneously equals 1.

The first requirement is satisfied if we impose the following conditions on F ($i,j,k=1,\ldots,n$):

$$F(\bar{0})=F(\widehat{\eta}_i)=0, \tag{15}$$

$$\partial F(\bar{0})/\partial \eta_i = \partial F(\widehat{\eta}_j)/\partial \eta_i = 0, \tag{16}$$

$$\partial F(\overline{\eta}_i)/\partial \eta_i = 0, \tag{17}$$

$$\partial^2 F(\bar{0})/\partial \eta_i^2 = \partial^2 F(\widehat{\eta}_i)/\partial \eta_i^2 = 0, \tag{18}$$

$$\partial^2 F(\bar{0})/\partial \eta_i \partial \eta_j = \partial^2 F(\widehat{\eta}_k)/\partial \eta_i \partial \eta_j = 0, \quad i \neq j. \tag{19}$$

Equation (15) preserves conditions (13) and (14). Equation (16) constrains $\bar{0}$ and $\widehat{\eta}_j$ to be extrema of the potential G. Equation (17) ensures that the $\partial G(\overline{\eta}_i)/\partial \eta_i$ are independent of F so that the $F=0$ equilibrium relations between the stress tensor, temperature, and η_i for each variant (in particular, equilibrium stress-strain curves) still hold. Equations (18) and (19) guarantee that the conditions for the $A \leftrightarrow M_i$ transformations are unchanged. Violation of conditions (19)

would lead to much more complex transformations. In particular, the transformations $A \leftrightarrow M_i$ would not occur along the path $\overline{\eta}_i$, $\eta_i \in [0,1]$.

For F a polynomial in the η_i, the minimal degree for which conditions (15)–(19) can be satisfied is fifth degree. Conditions (15)–(19) eliminate many terms from the full fifth-degree polynomial and impose proportionalities among the remaining terms. The result is

$$\begin{aligned} F_{ij} &= B\eta_i\eta_j^2 + C\eta_i^2\eta_j + D\eta_i^2\eta_j^2 - 2C\eta_i^3\eta_j - 2B\eta_i\eta_j^3 \\ &\quad + B\eta_i\eta_j^4 + C\eta_i^4\eta_j + (Y_{ij}-C-D)\eta_i^2\eta_j^3 \\ &\quad + (Z_{ij}-B-D)\eta_i^3\eta_j^2, \end{aligned} \tag{20}$$

where B, C, and D are constants and

$$\begin{aligned} 2Y_{ij} &= \partial^2 F_{ij}(\eta_i=0,\eta_j=1)/\partial \eta_i^2, \\ 2Z_{ij} &= \partial^2 F_{ij}(\eta_i=1,\eta_j=0)/\partial \eta_j^2. \end{aligned} \tag{21}$$

Invariance of F under interchange of indices i and j (see Sec. IV) implies the invariance of F_{ij}, which leads to

$$B=C, \quad Y_{ij}=Z_{ji}, \tag{22}$$

hence F_{ij} simplifies to

$$\begin{aligned} F_{ij} &= \eta_i\eta_j(1-\eta_i-\eta_j)\{B[(\eta_i-\eta_j)^2 - \eta_i - \eta_j] + D\eta_i\eta_j\} \\ &\quad + \eta_i^2\eta_j^2(\eta_i Z_{ij} + \eta_j Z_{ji}). \end{aligned} \tag{23}$$

Z_{ij} is chosen so that the condition for the $M_i \rightarrow M_j$ transformation, $\partial^2 G(\boldsymbol{\sigma},\theta,\widehat{\eta}_i)/\partial \eta_j^2 \leq 0$, coincides with Eq. (6) with indices 1 and 2 replaced by i and j, respectively;

$$Z_{ij}=\bar{A}-A+\boldsymbol{\sigma}{:}[(a-3)\boldsymbol{\varepsilon}_{tj}+3\boldsymbol{\varepsilon}_{ti}]. \tag{24}$$

In order to account for differences in elastic compliances and thermal expansion tensors among phases, we generalize the Gibbs potential $G(\boldsymbol{\sigma},\theta,\eta_1,\ldots,\eta_n)$ of Eq. (11)

$$\begin{aligned} G &= -\boldsymbol{\sigma}{:}\left(\boldsymbol{\lambda}_0 + \sum_{k=1}^{n}(\boldsymbol{\lambda}_k-\boldsymbol{\lambda}_0)[a_\lambda\eta_k^2+(4-2a_\lambda)\eta_k^3+(a_\lambda-3)\eta_k^4]\right){:}\boldsymbol{\sigma}/2 - \boldsymbol{\sigma}{:}\left[\left(\boldsymbol{\lambda}_0^3 + \sum_{k=1}^{n}(\boldsymbol{\lambda}_k^3-\boldsymbol{\lambda}_0^3)[a_{3\lambda}\eta_k^2+(4-2a_{3\lambda})\eta_k^3\right.\right. \\ &\quad \left.\left. + (a_{3\lambda}-3)\eta_k^4]\right){:}\boldsymbol{\sigma}\right]{:}\boldsymbol{\sigma}/3 - \boldsymbol{\sigma}{:}\left[\boldsymbol{\sigma}{:}\left(\boldsymbol{\lambda}_0^4 + \sum_{k=1}^{n}(\boldsymbol{\lambda}_k^4-\boldsymbol{\lambda}_0^4)[a_{4\lambda}\eta_k^2+(4-2a_{4\lambda})\eta_k^3+(a_{4\lambda}-3)\eta_k^4]\right){:}\boldsymbol{\sigma}\right]{:}\boldsymbol{\sigma}/4 \\ &\quad - \boldsymbol{\sigma}{:}\sum_{k=1}^{n}\boldsymbol{\varepsilon}_{tk}[a\eta_k^2+(4-2a)\eta_k^3+(a-3)\eta_k^4] - \boldsymbol{\sigma}{:}\left(\boldsymbol{\varepsilon}_{\theta 0} + \sum_{k=1}^{n}(\boldsymbol{\varepsilon}_{\theta k}-\boldsymbol{\varepsilon}_{\theta 0})[a_\theta\eta_k^2+(4-2a_\theta)\eta_k^3+(a_\theta-3)\eta_k^4]\right) \\ &\quad + \sum_{k=1}^{n}[A\eta_k^2+(4\Delta G^\theta-2A)\eta_k^3+(A-3\Delta G^\theta)\eta_k^4] + \sum_{i=1}^{n-1}\sum_{j=i+1}^{n}F_{ij}(\eta_i,\eta_j). \end{aligned} \tag{25}$$

The function Z_{ij} is obtained from the condition for the $M_i \rightarrow M_j$ transformation, $\partial^2 G(\boldsymbol{\sigma},\theta,\widehat{\eta}_i)/\partial \eta_j^2 \leq 0$ by requiring that it coincides with Eq. (10) with indices 1 and 2 replaced by i and j, respectively,

$$Z_{ij}=\bar{A}-A+\boldsymbol{\sigma}{:}[(a-3)\boldsymbol{\varepsilon}_{tj}+3\boldsymbol{\varepsilon}_{ti}]+\boldsymbol{\sigma}{:}[a_{\theta}(\boldsymbol{\varepsilon}_{\theta j}-\boldsymbol{\varepsilon}_{\theta 0})$$

$$-3(\boldsymbol{\varepsilon}_{\theta j}-\boldsymbol{\varepsilon}_{\theta i})]+\boldsymbol{\sigma}{:}[a_{\lambda}(\boldsymbol{\lambda}_j-\boldsymbol{\lambda}_0)-3(\boldsymbol{\lambda}_j-\boldsymbol{\lambda}_i)]{:}\boldsymbol{\sigma}/2$$

$$+\{\boldsymbol{\sigma}{:}[a_{3\lambda}(\boldsymbol{\lambda}_j^3-\boldsymbol{\lambda}_0^3)-3(\boldsymbol{\lambda}_j^3-\boldsymbol{\lambda}_i^3)]{:}\boldsymbol{\sigma}\}{:}\boldsymbol{\sigma}/3$$

$$+\boldsymbol{\sigma}{:}\{\boldsymbol{\sigma}{:}[a_{4\lambda}(\boldsymbol{\lambda}_j^4-\boldsymbol{\lambda}_0^4)-3(\boldsymbol{\lambda}_j^4-\boldsymbol{\lambda}_i^4)]{:}\boldsymbol{\sigma}\}{:}\boldsymbol{\sigma}/4. \quad (26)$$

Our complete Landau model is given by Eqs. (23), (25), and (26).

The transformation strain is a fifth-degree polynomial in the order parameters

$$\boldsymbol{\varepsilon}_t=\sum_{i=1}^n \boldsymbol{\varepsilon}_{ti}[a\eta_i^2+(4-2a)\eta_i^3+(a-3)\eta_i^4]$$

$$-\sum_{i=1}^{n-1}\sum_{j=i+1}^n \eta_i^2\eta_j^2[3(\eta_i\boldsymbol{\varepsilon}_{ti}+\eta_j\boldsymbol{\varepsilon}_{tj})$$

$$+(a-3)(\eta_i\boldsymbol{\varepsilon}_{tj}+\eta_i\boldsymbol{\varepsilon}_{tj})]. \quad (27)$$

It is easily verified that $\boldsymbol{\varepsilon}_t$ satisfies all requirements $\boldsymbol{\varepsilon}_t(\bar{0})=0$, $\boldsymbol{\varepsilon}_t(\hat{\eta}_i)=\boldsymbol{\varepsilon}_{ti}$, $\boldsymbol{\varepsilon}_t(\bar{\eta}_i)=\boldsymbol{\varepsilon}_{ti}\varphi(\eta_i)$.

[remainder of text omitted]

FIG. 1. Level curves of the function $\tilde{G}$ for $\theta = \theta_e = 200$ K and $D = -650$: (a) $\bar{A} = 300$, $\sigma = 0$; (b) $\bar{A} = 300$, $\sigma = -500$; (c) $\bar{A} = 300$, $\sigma = 1000$; (d) $\bar{A} = 600$, $\sigma = 1000$.

temperature is slightly reduced, thus preventing the $M_2 \rightarrow A$ and $M_1 \rightarrow A$ PT, then a barrier between variants M_1 and M_2 does exist.

At $\sigma = 1000$, A, and M_1 are stable, they are in thermodynamic equilibrium, and they are separated by a barrier; M_2 is unstable [Fig. 2(b)]. If the material is in state M_2 and the stress $\sigma = 1000$ is applied suddenly then a PT to either A or M_1 is possible. The final phase is contingent on the time dependence of the local stress during the transformation process. For $\sigma = 500$, M_2 is unstable in the A direction ($\partial^2 G / \partial \eta_2^2 \leqslant 0$) but not in the M_1 direction ($\partial^2 G / \partial \eta_1^2 \geqslant 0$) [Fig. 2(c)]. However, there is a path in the $\eta_1 \eta_2$ plane connecting M_2 and M_1 along which the free energy of the system decreases. Therefore, despite the fact that the energy minimum corresponding to A is significantly lower than for M_1, it is possible that transformation to M_1 rather than to A occurs because of stress fluctuations during the transformation process.

In Fig. 3, $\bar{A} = 900$ and $D = -1250$. For $\theta = 250$, and $\sigma = 1500$ [Fig. 3(a)], the conditions for $M_2 \rightarrow A$ and $A \rightarrow M_1$ are met, but the $M_2 \rightarrow M_1$ criterion is not fulfilled. Although the criterion for the $M_2 \rightarrow M_1$ transition is not fulfilled, the $M_2 \rightarrow M_1$ transformation will occur via phase A or along some path passing near A.

If the temperature and stress are reduced to $\theta = 230$ and $\sigma = 250$ [Fig. 3(b)], then variant M_2 loses its stability in direction M_1 ($\partial^2 G / \partial \eta_1^2 \leqslant 0$), but not in direction A ($\partial^2 G / \partial \eta_2^2 \geqslant 0$). However, since G at A is lower than at M_1, stress fluctuations during transformation lead to A with a higher probability than to M_1. Hence there is some conventionality in the statement that $\partial^2 G(0,1) / \partial \eta_1^2 \leqslant 0$ is the $M_2 \rightarrow M_1$ PT criterion, while $\partial^2 G(0,1) / \partial \eta_2^2 \leqslant 0$ is the $M_2 \rightarrow A$ PT condition. Either of these conditions leads to loss of stability of M_2 and the phase reached depends on the solution of the dynamic boundary-value problem.

The Landau model developed here remains valid if the temperature dependences of the material tensors are in
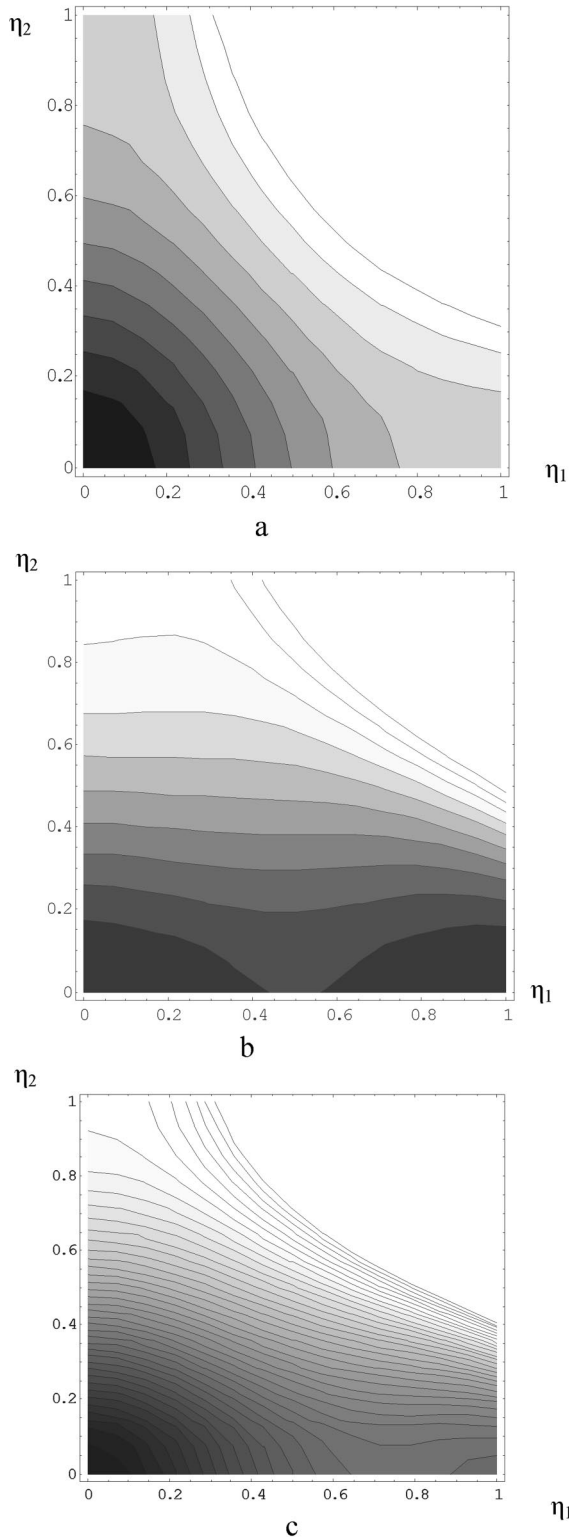
FIG. 2. Level curves of the function $\tilde{G}$ at three stresses σ for $\theta = \bar{\theta}_c = 300$ K, $\bar{A} = 300$, and $D = -1250$: (a) $\sigma = 0$; (b) $\sigma = 1000$; (c) $\sigma = 500$.

FIG. 3. Level curves of the function $\tilde{G}$ for $D = -1250$ and $\bar{A} = 900$: (a) $\theta = 250$ K, $\sigma = 1500$; (b) $\theta = 230$ K, $\sigma = 250$.

rial parameters can be taken from experiments or molecular dynamics simulations.

IV. SYMMETRIES OF THE GIBBS POTENTIAL

The Gibbs potential G possesses both point group and permutation symmetries. First, the tensors $\boldsymbol{\lambda}_0$, $\boldsymbol{\varepsilon}_{\theta 0}$ and the tensors $\boldsymbol{\lambda}_i$, $\boldsymbol{\varepsilon}_{\theta i}$ appearing in G are invariant under transformations of P_A and P_M, respectively. Second, by definition of martensitic variants, $\boldsymbol{\varepsilon}_{ti} = \boldsymbol{R} \cdot \boldsymbol{\varepsilon}_{tj} \cdot \boldsymbol{R}^t$ with some orthogonal tensor $\boldsymbol{R}$ from P_A. Thus, products of P_A transformations lead to permutation of the martensitic variants. Consequently, invariance of G under P_A implies invariance of G

cluded. For example, one can introduce $\boldsymbol{\varepsilon}_{ti}(\theta)$ with $\boldsymbol{\varepsilon}_{ti}(\theta_e) \boldsymbol{\varepsilon}_{ti}(\theta_e) = 0$ in order to describe ferroelastic materials. In that case our Gibbs potential will be more realistic than in Ref. 2 because it is a three-dimensional model and all mate-

under all permutations of the indices $i \leftrightarrow j$ or, more precisely, with respect to all permutations $(\varepsilon_{ti}, \boldsymbol{\lambda}_i, \boldsymbol{\varepsilon}_{\theta i}, \eta_i) \leftrightarrow (\varepsilon_{tj}, \boldsymbol{\lambda}_j, \boldsymbol{\varepsilon}_{\theta j}, \eta_j)$, which is the case for our Gibbs potential (11). This is not the most general potential invariant under point group symmetries (for example, terms involving more than two order parameters, such as $\eta_1^k \eta_2^m \eta_3^n$, are absent), but it is the simplest polynomial potential that satisfies all the requisite conditions discussed above. More complex potentials might violate these conditions, significantly complicate the formulation of the transformation conditions, or possess unphysical extrema. Following standard practice we adopt the simplest possible polynomial expression for the chemical part of the Gibbs energy.[2–11]

Our Gibbs potential does not possess inversion symmetry, i.e. it is not an even function of the transformation strain. Nevertheless, the stress-strain curves for multivariant PT can be symmetric under inversion. Consider the simplest case, namely, the one-dimensional loading of a material that has two martensitic variants with $\varepsilon_{t2} = -\varepsilon_{t1}$. It is easy to show that the stress-strain curves for negative stresses can be obtained by inversion of the curves for positive stresses through the point $\sigma = \varepsilon = 0$; see Fig. 1 in part I.[1]

V. PHASE EQUILIBRIUM AND TRANSFORMATION DIAGRAMS IN STRESS SPACE

The conditions for thermodynamic equilibrium and the sequence of phases appearing along arbitrarily complicated loading paths can be conveniently analyzed by reference to equilibrium and transformation surfaces in stress space. In this section we develop this methodology for the case of equal compliances for A and M_i, and negligible thermal strain and higher-order elastic constants, and apply it specifically to the cubic to tetragonal transformation.

We define the six-dimensional stress vector $\overline{\boldsymbol{\sigma}} = \{\sigma^{11}, \sigma^{22}, \sigma^{33}, \sqrt{2}\sig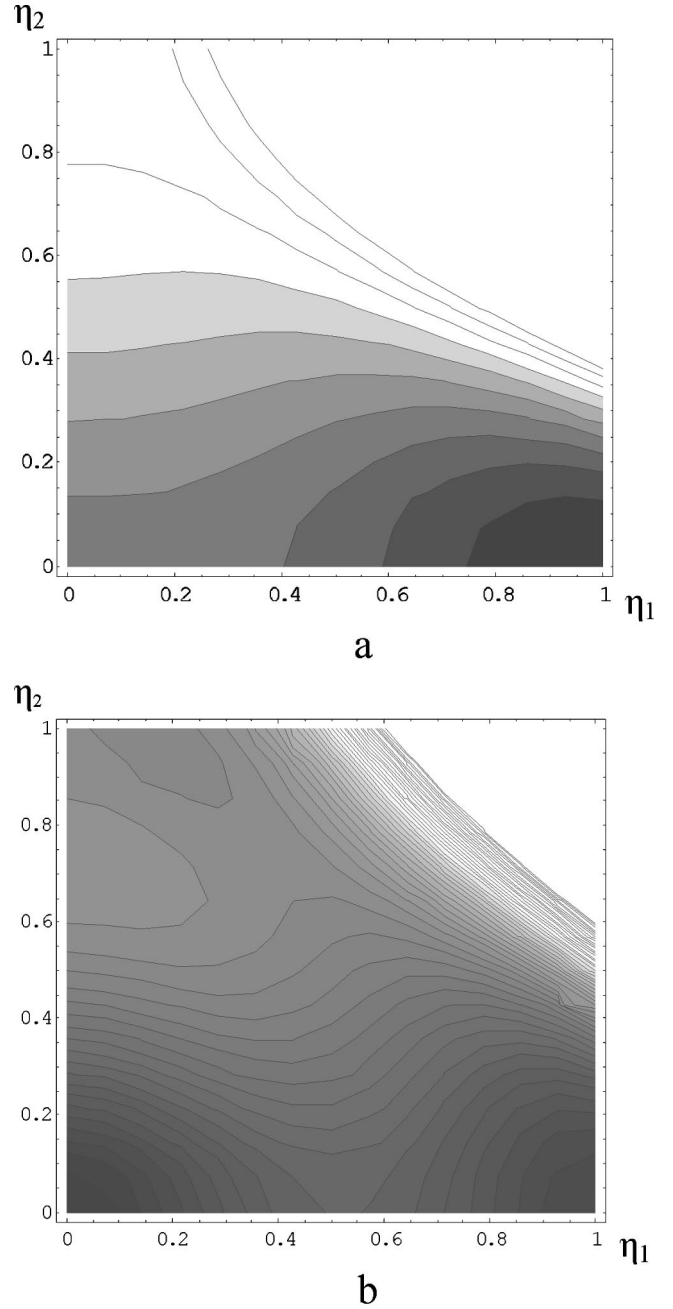ma^{23}, \sqrt{2}\sigma^{13}, \sqrt{2}\sigma^{12}\}$ and transformation strain vectors $\overline{\boldsymbol{\varepsilon}}_{ti} = \{\varepsilon_{ti}^{11}, \varepsilon_{ti}^{22}, \varepsilon_{ti}^{33}, \sqrt{2}\varepsilon_{ti}^{23}, \sqrt{2}\varepsilon_{ti}^{13}, \sqrt{2}\varepsilon_{ti}^{12}\}$. The factors of $\sqrt{2}$ are introduced so that the tensor and vector norms are equal: $(\boldsymbol{\sigma} : \boldsymbol{\sigma})^{1/2} = (\overline{\boldsymbol{\sigma}} \cdot \overline{\boldsymbol{\sigma}})^{1/2}$ and $(\boldsymbol{\varepsilon}_{ti} : \boldsymbol{\varepsilon}_{ti})^{1/2} = (\overline{\boldsymbol{\varepsilon}}_{ti} \cdot \overline{\boldsymbol{\varepsilon}}_{ti})^{1/2}$. The relation $\boldsymbol{\sigma} : \boldsymbol{\varepsilon}_{ti} = \sum_{k=1}^3 \sum_{l=1}^3 \sigma^{kl} \varepsilon_{ti}^{kl} = \sum_{m=1}^6 \sigma^m \varepsilon_{ti}^m = \overline{\boldsymbol{\sigma}} \cdot \overline{\boldsymbol{\varepsilon}}_{ti}$ allows us to replace the double contraction of stress and transformation-strain tensors by inner products of stress and transformation-strain vectors. Henceforth we drop the bar over vectors and use the same symbol for tensors and vectors.

A. Phase equilibrium surfaces

According to Eqs. (13) and (14), thermodynamic equilibrium between phases is described by the conditions

$$A - M_i: \quad \boldsymbol{\sigma} \cdot \boldsymbol{\varepsilon}_{ti} - \Delta G^\theta = 0, \tag{31}$$

$$M_i - M_j: \quad \boldsymbol{\sigma} \cdot (\boldsymbol{\varepsilon}_{ti} - \boldsymbol{\varepsilon}_{tj}) = 0. \tag{32}$$

In stress space, the stress vectors described by Eq. (31) for each i belong to the hyperplane orthogonal to the vector $\boldsymbol{\varepsilon}_{ti}$ and shifted by distance $\Delta G^\theta / |\varepsilon_{ti}|$ in the $\boldsymbol{\varepsilon}_{ti}$ direction from the origin O of the coordinate system. The stress vectors de-

scribed by Eq. (32) for each i and j belong to the hyperplane through the origin and orthogonal to the vector $\boldsymbol{\varepsilon}_{ti} - \boldsymbol{\varepsilon}_{tj}$. All such planes divide stress space into $n+1$ subspaces, in each of which one of the phases is stable. The following inequalities determine the region of stability of each phase:

$$\text{stability of } A: \quad \boldsymbol{\sigma} \cdot \boldsymbol{\varepsilon}_{ti} \leqslant \Delta G^\theta, \tag{33}$$

$$\text{stability of } M_i: \quad \boldsymbol{\sigma} \cdot \boldsymbol{\varepsilon}_{ti} \geqslant \Delta G^\theta \text{ and } \boldsymbol{\sigma} \cdot (\boldsymbol{\varepsilon}_{ti} - \boldsymbol{\varepsilon}_{tj}) \geqslant 0 \quad \forall j$$
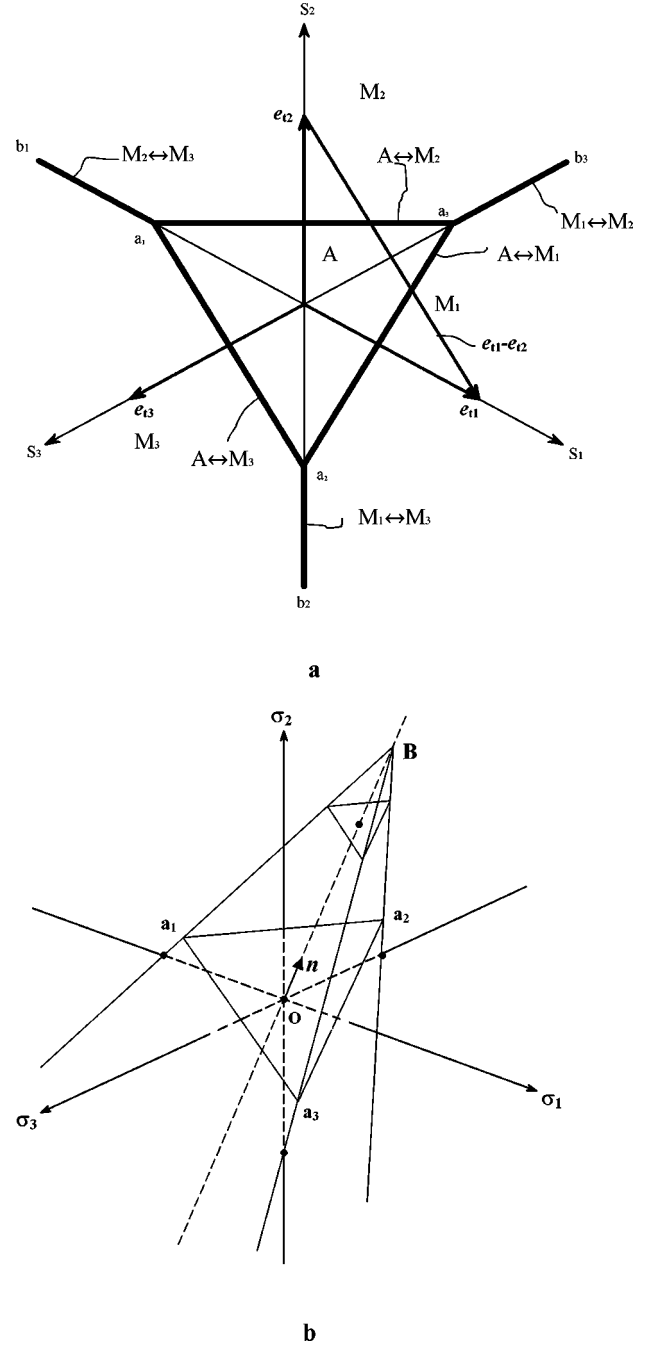$$\neq i. \tag{34}$$

FIG. 4. Equilibrium phase diagram for the cubic-tetragonal phase transformation (a) in the deviatoric-stress plane and (b) in the stress space at $\theta > \theta_e$.
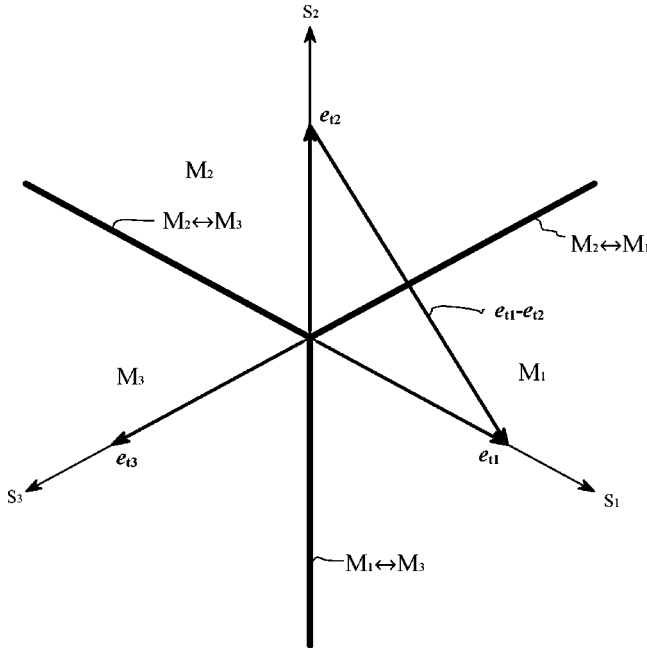
FIG. 5. Equilibrium phase diagram for the cubic-tetragonal phase transformation in the deviatoric-stress plane at $\theta < \theta_e$.

Phase equilibrium in the general six-dimensional case is most easily investigated by decomposing the stress tensor into spherical $\sigma_0 I$ and deviatoric S parts $\boldsymbol{\sigma} = \sigma_0 I + S$, where $\sigma_0 = \frac{1}{3} I : \boldsymbol{\sigma} = \frac{1}{3}(\sigma^{11} + \sigma^{22} + \sigma^{33})$ is the mean stress (negative pressure), and I is the second-rank unit tensor. Transformation strains are likewise decomposed: $\boldsymbol{\varepsilon}_{ti} = \frac{1}{3}\varepsilon_0 I + e_{ti}$, where $\varepsilon_0 = \varepsilon_{ti}^{11} + \varepsilon_{ti}^{22} + \varepsilon_{ti}^{33}$ is the volumetric transformation strain which is the same for all variants. It is evident that $I : S = I : e_{ti} = 0$, hence

$$\boldsymbol{\sigma} \cdot \boldsymbol{\varepsilon}_{ti} = \sigma_0 \varepsilon_0 + S \cdot e_{ti}, \tag{35}$$

where the deviator vectors are

$$S = \{\sigma^{11} - \sigma_0, \sigma^{22} - \sigma_0, \sigma^{33} - \sigma_0, \sqrt{2}\sigma^{23}, \sqrt{2}\sigma^{13}, \sqrt{2}\sigma^{12}\}, \tag{36}$$

$$e_{ti} = \left\{ \varepsilon_{ti}^{11} - \frac{1}{3}\varepsilon_0, \varepsilon_{ti}^{22} - \frac{1}{3}\varepsilon_0, \varepsilon_{ti}^{33} \right.$$
$$\left. - \frac{1}{3}\varepsilon_0, \sqrt{2}\varepsilon_{ti}^{23}, \sqrt{2}\varepsilon_{ti}^{13}, \sqrt{2}\varepsilon_{ti}^{12} \right\}. \tag{37}$$

In terms of the deviator vectors, the equilibrium and stability conditions (31)–(34) are

$$A - M_i: \quad S \cdot e_{ti} = \Delta G^\theta - \sigma_0 \varepsilon_0,$$
$$M_i - M_j: \quad S \cdot (e_{ti} - e_{tj}) = 0, \tag{38}$$

$$\text{stability of } A: \quad S \cdot e_{ti} \leq \Delta G^\theta - \sigma_0 \varepsilon_0, \tag{39}$$

$$\text{stability of } M_i: \quad S \cdot e_{ti} \geq \Delta G^\theta - \sigma_0 \varepsilon_0, \text{ and } S \cdot (e_{ti} - e_{tj})$$
$$\geq 0 \quad \forall j \neq i. \tag{40}$$

The pure hydrostatic stress state and the pure volumetric strain state can be represented by vectors $\sigma_0 \boldsymbol{n}$ and $\frac{1}{3}\varepsilon_0 \boldsymbol{n}$ with unit vector $\boldsymbol{n} = \{1,1,1,0,0,0\}/\sqrt{3}$ that is directed along the so-called hydrostatic axis in stress space. Since $\boldsymbol{n} \cdot S = \boldsymbol{n} \cdot e_{ti} = 0$, the vectors S and e_{ti} belong to the five-dimensional deviatoric plane $\boldsymbol{n} \cdot \boldsymbol{\sigma} = 0$ which passes through the origin O and is orthogonal to the hydrostatic axis.

As an example that can be easily visualized we consider the cubic-tetragonal PT. The three martensitic variants can be described by the three transformation-strain vectors

$$\boldsymbol{\varepsilon}_{t1} = \alpha \boldsymbol{i}_1 + \beta \boldsymbol{i}_2 + \beta \boldsymbol{i}_3, \quad \boldsymbol{\varepsilon}_{t2} = \beta \boldsymbol{i}_1 + \alpha \boldsymbol{i}_2 + \beta \boldsymbol{i}_3,$$
$$\boldsymbol{\varepsilon}_{t3} = \beta \boldsymbol{i}_1 + \beta \boldsymbol{i}_2 + \alpha \boldsymbol{i}_3, \tag{41}$$

where the $\boldsymbol{i}_k$ are orthonormal basis vectors and α and β are principal transformation strains. Since only the normal stress σ^{kk} induces the PT the stress vector is $\boldsymbol{\sigma} = \Sigma_{k=1}^3 \sigma^{kk} \boldsymbol{i}_k$. Thus the cubic-tetragonal PT can be analyzed in three-dimensional space. The transformation deviators for the cubic-tetragonal PT are

$$e_{t1} = \varepsilon \left(\boldsymbol{i}_1 - \frac{1}{2}\boldsymbol{i}_2 - \frac{1}{2}\boldsymbol{i}_3 \right), \quad e_{t2} = \varepsilon \left(-\frac{1}{2}\boldsymbol{i}_1 + \boldsymbol{i}_2 - \frac{1}{2}\boldsymbol{i}_3 \right),$$
$$e_{t3} = \varepsilon \left(-\frac{1}{2}\boldsymbol{i}_1 - \frac{1}{2}\boldsymbol{i}_2 + \boldsymbol{i}_3 \right), \tag{42}$$

where $\varepsilon := 2(\alpha - \beta)/3$. The projections of the unit vectors $\boldsymbol{i}_i$ on the deviatoric plane, $s_i := \boldsymbol{i}_i - \boldsymbol{i}_i \cdot \boldsymbol{n}\boldsymbol{n}$, are parallel to the transformation strain deviators $s_i = (2/3\varepsilon)e_{ti}$. It is easy to show that $e_{tk} \cdot (e_{tl} - e_{tm}) = s_k \cdot (e_{tl} - e_{tm}) = 0$ for $k \neq l \neq m$ [Fig. 4(a)].

We first analyze cubic-tetragonal equilibrium in the deviatoric plane $\boldsymbol{n} \cdot \boldsymbol{\sigma} = 0$, that is for $\sigma_0 = (\sigma^{11} + \sigma^{22} + \sigma^{33})/3 = 0$; see Fig. 4(a). Consider the case $\theta > \theta_e$, i.e., $\Delta G^\theta > 0$. Equation (39) holds inside the triangle $a_1 a_2 a_3$ which is the region of stability of A. Lines of constant σ^{ii} are orthogonal to s_i, hence parallel to the sides of the triangle. The distance between O and the side of the triangle is $\sqrt{2/3}\Delta G^\theta/\varepsilon$ [$\sqrt{e_{ti} \cdot e_{ti}} = \sqrt{3/2}\varepsilon$, see Eq. (42)] which corresponds to $\sigma^{ii} = 2\Delta G^\theta/3\varepsilon$ (follows from geometrical considerations). The second set of inequalities (40) for M_i describe a sector with apex at O which includes the vector $\boldsymbol{\varepsilon}_{ti}$, does not include any other transformation strain vectors, and is unbounded in the direction of $\boldsymbol{\varepsilon}_{ti}$. The first set of inequalities (40) eliminate the region of stability of A from the sector, hence the stability regions of M_1, M_2, and M_3 are the convex regions bounded by $b_2 a_2 a_3 b_3$, $b_1 a_1 a_3 b_3$, and $b_2 a_2 a_1 b_1$. With decreasing temperature, the region of stability of A shrinks and disappears at $\theta = \theta_e$ (Fig. 5). It does not exist for $\theta < \theta_e$ either, because Eqs. (39) do not have a solution, which can be checked graphically. Moreover, for $\Delta G^\theta < 0$, the line of A-M_i equilibrium does not intersect the positive s_i axis and is outside the region of M_i stability. Consequently, there is no A-M_i equilibrium for $\theta < \theta_e$ and the equilibrium diagram is the same as at $\theta = \theta_e$.

In planes parallel to the deviatoric plane ($\sigma_o \neq 0$) the region of stability of A is simply rescaled—the distance be-
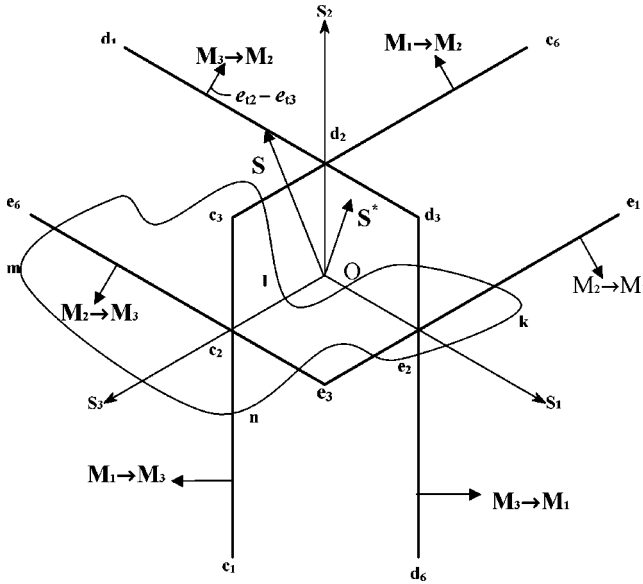
FIG. 6. Phase transformation diagram for low temperatures where austenite does not exist. Pseudoplasticity arises from reorientation processes only.

tween the center and the side of the triangle is $\sqrt{2/3}(\Delta G^\theta - \sigma_0 \varepsilon_0)/\varepsilon$. In the three-dimensional stress space of the cubic-tetragonal PT, which is depicted in Fig. 4(b), the region of stability of A is a triangular pyramid with base at infinity, apex B on the hydrostatic axis corresponding to $\sigma_0 = \Delta G^\theta / \varepsilon_0$, and edges that intersect the axes at $-3\Delta G^\theta / [(3/2)^{3/2} \varepsilon - \varepsilon_0]$. For A stable, the M_i-M_j equilibrium half-planes are attached to the edges of the pyramid and contain the negative parts of the σ^k axes; when A is unstable, they are attached to the hydrostatic axis.

The geometric analysis of cubic-tetragonal phase equilibria, which involves three variants and $\boldsymbol{\varepsilon}_{ti}$ with equal magnitudes, can be generalized to an arbitrary number n of martensitic variants with arbitrary $\boldsymbol{\varepsilon}_{ti}$. For $\theta > \theta_e$ and $\sigma_0 = 0$, the stability region of A in the five-dimensional deviatoric hyperplane is a five-dimensional prism with an n-sided polygonal base which includes O. The stability region of M_i is a truncated pyramid defined by inequalities (40). The second set of inequalities (40) describe a pyramid with an $n-1$-sided polygonal base at infinity with apex at O. The pyramid includes the vector $\boldsymbol{e}_{ti}$, does not include any of the other $\boldsymbol{e}_{tj}$, and is unbounded in the $\boldsymbol{e}_{ti}$ direction. The first set of inequalities (40) remove a region of austenite stability from the apex of the pyramid. With decreasing temperature, the region of stability of A shrinks to a point at $\theta = \theta_e$ and does not exist for $\theta < \theta_e$.

As in the cubic to tetragonal case, the region of stability of A rescales in planes parallel to the deviatoric plane. In the six-dimensional stress space, the region of stability of A is a pyramid with an n-sided polygonal base at infinity and apex on the hydrostatic axis corresponding to the pressure $\sigma_0 = \Delta G^\theta / \varepsilon_0$.

B. Phase transformation surfaces

The conditions for phase transformations, Eqs. (4) and (5), can be written as

a

b
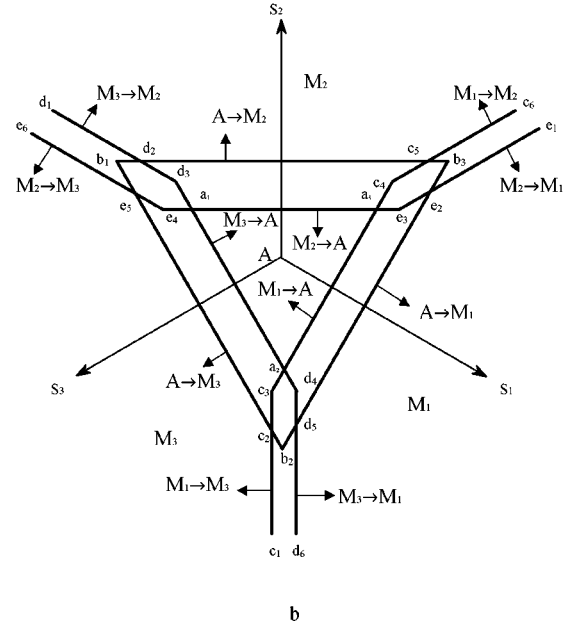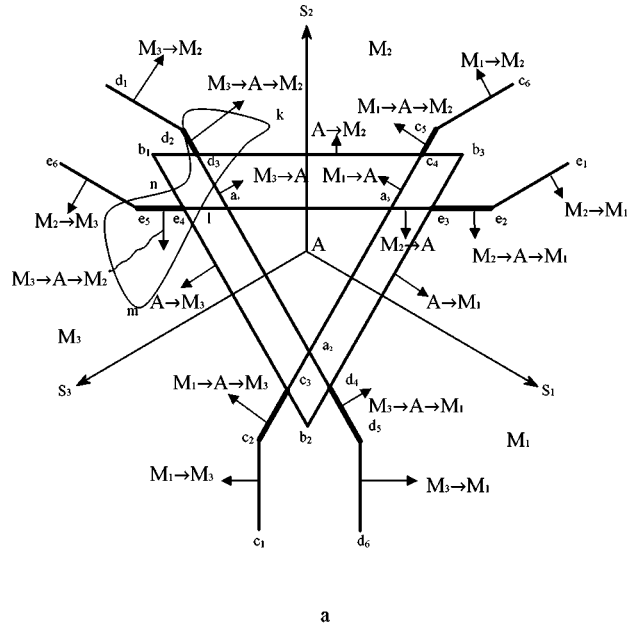
FIG. 7. Phase transformation diagram for coexisting austenite and martensitic variants in the pseudoelastic regime. Stress hysteresis for the phase transformation $A \leftrightarrow M_i$ is (a) smaller than for reorientation $M_i \leftrightarrow M_j$, and (b) larger than for reorientation.

$$A \rightarrow M_i: \quad \boldsymbol{S} \cdot \boldsymbol{e}_{ti} \geqslant \frac{A}{a} - \sigma_0 \varepsilon_0,$$

$$M_i \rightarrow A: \quad \boldsymbol{S} \cdot \boldsymbol{e}_{ti} \leqslant \frac{6\Delta G^\theta - A}{6-a} - \sigma_0 \varepsilon_0, \qquad (43)$$

$$M_l \rightarrow M_k: \quad \boldsymbol{S} \cdot (\boldsymbol{e}_{tk} - \boldsymbol{e}_{tl}) \geqslant \frac{\bar{A}}{3}.$$

It follows from these equations that stress space is subdivided by transformation planes of three types: $A \leftrightarrow M_i$

FIG. 8. Phase transformation diagram for the limiting case between pseudoelasticity and pseudoplasticity: the austenite triangle $a_1a_2a_3$ has contracted to the origin.

planes; double-PT planes (discussed below); and $M_i \leftrightarrow M_j$ planes. The $M_i \rightarrow M_j$ and $M_j \rightarrow M_i$ planes, which are always present, are parallel to and equidistant from the $M_i - M_j$ equilibrium plane. The $A \rightarrow M_i$ and $M_i \rightarrow A$ planes, when present, are parallel to each other. The separation of the $A \leftrightarrow M_i$ and $M_i \leftrightarrow M_j$ planes is proportional to the corresponding hysteresis.

We define the region of metastability of a given phase as that region outside of which the phase is absolutely unstable and cannot exist. The region of stability is included in the region of metastability. The conditions defining the regions of metastability of A and the M_i are

FIG. 9. Phase transformation diagram for coexisting austenite and martensitic variants. Pseudoplasticity is due to both the $A \leftrightarrow M_i$ phase transformation and the reorientations $M_i \leftrightarrow M_j$.
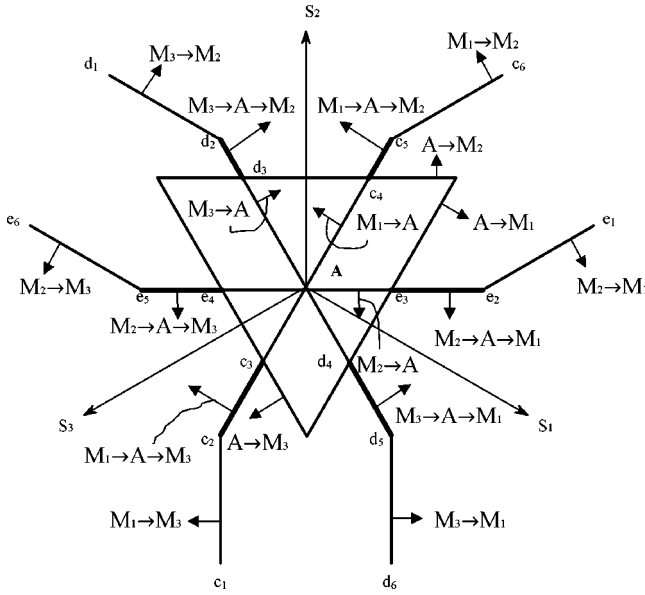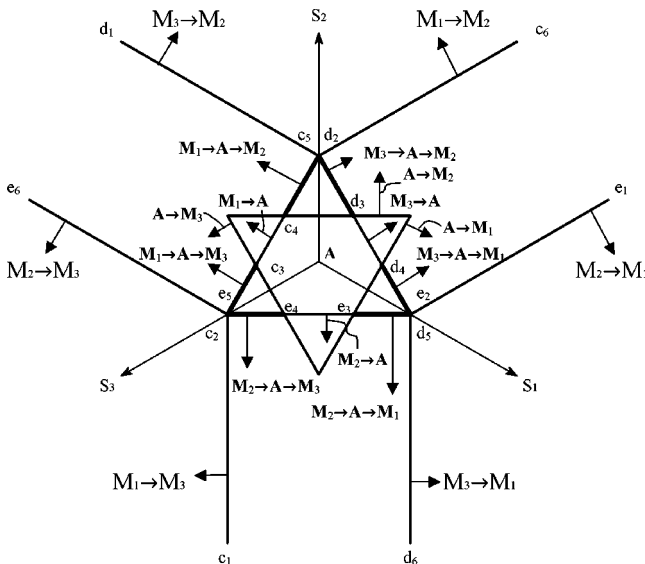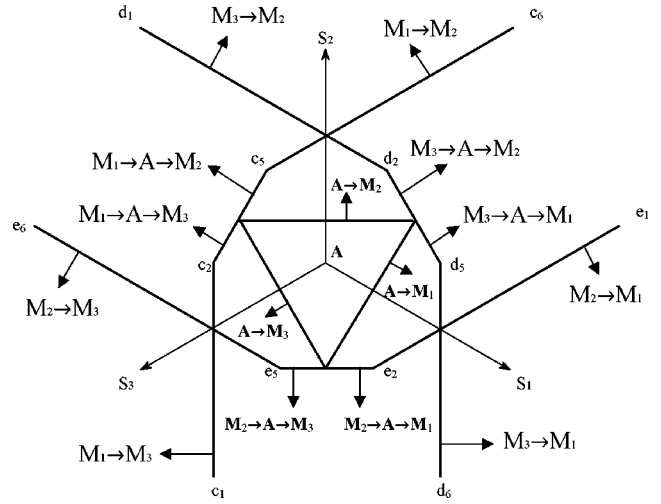

FIG. 10. Phase transformation diagram for coexisting austenite and martensitic variants. Transformations to austenite are absent, so pseudoplasticity is due solely to the reorientations $M_i \leftrightarrow M_j$.

metastability of A:$\qquad \boldsymbol{S} \cdot \boldsymbol{e}_{ti} \leqslant \dfrac{A}{a} - \sigma_0 \varepsilon_0,$

metastability of M_i:$\qquad \boldsymbol{S} \cdot \boldsymbol{e}_{ti} \geqslant \dfrac{6\Delta G^\theta - A}{6-a} - \sigma_0 \varepsilon_0 \;$ and

$$\boldsymbol{S} \cdot (\boldsymbol{e}_{tk} - \boldsymbol{e}_{ti}) \leqslant \frac{\bar{A}}{3} \forall k \neq i. \qquad (44)$$

Transformation diagrams in the deviatoric plane for the cubic-tetragonal PT for various temperatures and material parameter values are presented in Figs. 6–10.

The simplest diagram is for sufficiently low enough temperatures that transformations to and from A are absent (Fig. 6). This corresponds to pseudoplasticity due to reorientation processes. Each transformation line is parallel to the corresponding equilibrium line and shifted from it by $\sqrt{2}\bar{A}/(9\varepsilon)$ $[\sqrt{(\boldsymbol{e}_{ti} - \boldsymbol{e}_{tk}) \cdot (\boldsymbol{e}_{ti} - \boldsymbol{e}_{tk})} = 3\varepsilon/\sqrt{2}$, see Eq. (42)]. Arrows indicate the direction in which the transformation line has to be crossed in order for the corresponding PT to occur. Only variant M_1, M_2, or M_3 exists in the nonconcave region $e_1e_2d_6$, $d_1d_2c_6$, or $c_1c_2e_6$, respectively. Variant M_1 does not exist outside the nonconcave region $c_1c_3c_6$, its region of metastability, because it transforms either to M_2 along the line c_3c_6 or to M_3 along c_1c_3. Likewise, variant M_2 (M_3) does not exist outside the nonconcave region $e_1e_3e_6$ ($d_1d_3d_6$). Thermomechanical history determines which variant exists at a given point. Progressing along the path $klmnk$ from the point k where only M_1 can exist, the $M_1 \rightarrow M_2$ PT occurs where the path crosses the line c_3d_2, the $M_2 \rightarrow M_3$ PT occurs at the line e_6c_2, and the $M_3 \rightarrow M_1$ PT occurs at the line d_6e_2. Proceeding in the opposite direction from k, the $M_1 \rightarrow M_3$ PT occurs at the line c_1c_2, and the $M_3 \rightarrow M_1$ PT takes place at the line e_2d_3. A PT occurs at a transformation line if and only if the line is crossed in the direction of the corresponding arrow and the material is in the initial phase for this transformation. Note that any variant may exist inside the hexagon $c_2c_3d_2d_3e_2e_3$ depending on history. It

makes no sense to continue the line $c_6 c_3$ further than the point c_3—this portion of the $M_1 \rightarrow M_2$ transformation line is physically irrelevant because the material has already transformed to M_3 along the line $c_1 c_3$. Each of the remaining five $M_i \rightarrow M_j$ lines are similarly truncated.

In Fig. 7 a much more complex transformation diagram is shown for the pseudoelastic regime, i.e., where unloading results in only A. In Fig. 7(a) the hysteresis for $M_i \leftrightarrow M_j$ is larger than for $A \leftrightarrow M_i$; vice versa in Fig. 7(b). In addition to lines of $M_i \rightarrow M_j$ PT ($d_1 d_3$, $e_4 e_6$, $c_1 c_3$, $d_4 d_6$, $e_1 e_3$, and $c_4 c_6$), lines of $A \rightarrow M_i$ PT ($b_1 b_2$, $b_2 b_3$, and $b_3 b_1$), and lines of $M_i \rightarrow A$ PT ($c_3 c_4$, $d_3 d_4$, and $e_3 e_4$) are present. An interesting feature of Fig. 7(a) that is absent from Fig. 7(b) is the "double" PT along the lines $c_2 c_3$, $d_4 d_5$, $e_2 e_3$, $c_4 c_5$, $d_2 d_3$, and $e_4 e_5$. For example, the $M_1 \rightarrow A$ PT occurs along the line segment $c_2 c_3$ but A is unstable in this region with respect to M_3 (outside the line $b_1 b_2$ A transforms to M_3), hence the $A \rightarrow M_3$ PT occurs immediately. Consequently, despite the fact that the direct $M_1 \rightarrow M_3$ PT is impossible along the line $c_2 c_3$, the "double" PT $M_1 \rightarrow A \rightarrow M_3$ can occur. This situation is similar to the one analyzed in Fig. 3(a). Inside the triangle $a_1 a_2 a_3$ only A can exist.

In the region $e_1 e_2 e_3 d_4 d_5 d_6$, $d_1 d_2 d_3 c_4 c_5 c_6$, or $c_1 c_2 c_3 e_4 e_5 e_6$, there exists, respectively, only the variant M_1, M_2, or M_3. A does not exist outside $b_1 b_2 b_3$, its region of metastability, because it transforms to one of the martensitic variants along the sides of the triangle. The nonconcave region $c_1 c_2 c_3 c_4 c_5 c_6$ is the region of metastability of variant M_1 because it transforms either to M_2 along the line $c_4 c_5 c_6$, or to M_3 along $c_1 c_2 c_3$, or to A along $c_3 c_4$. Similarly, variant M_2 (M_3) does not exist outside the nonconcave region $e_1 e_2 e_3 e_4 e_5 e_6$ ($d_1 d_2 d_3 d_4 d_5 d_6$).

Along the path $klmnk$ the $M_2 \rightarrow A$ PT occurs across $a_1 e_4$, the $A \rightarrow M_3$ PT occurs where it crosses $c_3 e_4$, and the $M_3 \rightarrow M_2$ PT takes place where the path crosses $d_1 d_2$. Along the path $knmlk$ the $M_2 \rightarrow M_3$ PT occurs at its intersection with $e_5 e_6$, the $M_3 \rightarrow A$ PT takes place where it crosses $a_1 d_3$, and the $A \rightarrow M_2$ PT occurs where it crosses $d_3 c_4$.

In Figs. 8–10 the hysteresis for the $M_i \leftrightarrow M_j$ PT is larger than for the $A \leftrightarrow M_i$ PT. Figure 8 represents the limiting case between pseudoelasticity and pseudoplasticity, that is, the triangle $a_1 a_2 a_3$ has contracted to O at a sufficiently low temperature. With a further decrease in temperature (Fig. 9), the $M_i \rightarrow A$ PT occurs at negative stresses, and common points appear along the transformation lines for $M_j \rightarrow M_i$ and $M_k \rightarrow M_i$ ($i \neq j \neq k$): d_2, c_5; c_2, e_5; and e_2, d_5. At lower temperatures (Fig. 10) there are no PT to A, i.e., the line segments $c_3 c_4$, $d_3 d_4$, and $e_3 e_4$ disappear.

We now consider loading processes along axis s_1. In order to avoid the appearance of M_3, motion is parallel to the s_1 axis at a positive infinitesimal value of s_2. In Fig. 7(a), loading begins at O (i.e., in A) in the positive s_1 direction. The $A \rightarrow M_1$ PT occurs at the intersection of the line $e_3 d_4$ with the axis s_1. Upon reverse loading the $M_1 \rightarrow A$ PT does not take place until the path intersects the line $a_2 a_3$, hence there is hysteresis. The PT $A \rightarrow M_2$ occurs at point b_1. If the $M_1 \rightarrow A$ PT were suppressed, then the $M_1 \rightarrow M_2$ PT would occur at the intersection of the line $c_5 c_6$ with the axis s_1, i.e.,

before the actual $A \rightarrow M_2$ PT. The $M_1 \rightarrow A$ PT delays the appearance of the M_2 variant. If point b_1 is closer to O than the intersection of the $M_1 \rightarrow M_2$ PT line with the axis s_1, then the M_2 variant appears earlier due to the double PT $M_1 \rightarrow A \rightarrow M_2$ (Fig. 10).

C. Associated transformation rule and principle of maximum transformation work

Transformation surfaces for $i \rightarrow j$ PT are specified by $q_{ji} = \boldsymbol{\sigma} \cdot (\boldsymbol{\varepsilon}_{tj} - \boldsymbol{\varepsilon}_{ti}) + \cdots = 0$, where $i, j = 0$ for A and $\cdots$ designates irrelevant stress-independent terms. The inequality $q_{ji} \geq 0$ corresponds to the occurrence of the $i \rightarrow j$ PT and the set of inequalities $q_{ji} < 0$ $\forall j \neq i$ defines the region of metastability for phase i.

There are similarities between phase equilibrium and transformation surfaces and yield surfaces in plasticity theory.[12] In both cases, such surfaces divide the stress space into regions where inelastic processes (PT or plasticity) occur and do not occur. In both cases, an increment of inelastic deformation, either an infinitesimal change in plastic strain or a finite jump in transformation strain, is orthogonal to the corresponding surface; this is the associated (with the yield surface) flow rule in plasticity theory. The associated transformation rule

$$\boldsymbol{\varepsilon}_{tj} - \boldsymbol{\varepsilon}_{ti} = \frac{\partial q_{ji}}{\partial \boldsymbol{\sigma}} \qquad (45)$$

follows trivially from $q_{ji} = \boldsymbol{\sigma} \cdot (\boldsymbol{\varepsilon}_{tj} - \boldsymbol{\varepsilon}_{ti}) + \cdots$.

It is seen from Figs. 6–10 that the region of metastability of each phase is nonconcave, i.e., if $\boldsymbol{\sigma}$ and $\boldsymbol{\sigma}^*$ belong to the metastability region then the difference $\boldsymbol{\sigma} \cdot \boldsymbol{\sigma}^*$ belongs as well. It is easy to prove geometrically (see Fig. 6) and analytically that for a nonconcave region of metastability the associated transformation rule is equivalent to the principle of maximum transformation work

$$\boldsymbol{\sigma} \cdot (\boldsymbol{\varepsilon}_{tj} - \boldsymbol{\varepsilon}_{ti}) > \boldsymbol{\sigma}^* \cdot (\boldsymbol{\varepsilon}_{tj} - \boldsymbol{\varepsilon}_{ti}) \quad \text{for} \quad q_{ji}(\boldsymbol{\sigma}) = 0$$

$$\text{and} \quad q_{ji}(\boldsymbol{\sigma}^*) < 0, \quad \boldsymbol{\sigma} \cdot (\boldsymbol{\varepsilon}_{tj} - \boldsymbol{\varepsilon}_{ti}) = \boldsymbol{\sigma}^* \cdot (\boldsymbol{\varepsilon}_{tj} - \boldsymbol{\varepsilon}_{ti})$$

$$\text{for} \quad q_{ji}(\boldsymbol{\sigma}) = q_{ji}(\boldsymbol{\sigma}^*) = 0, \qquad (46)$$

that is, the transformation work done by a $\boldsymbol{\sigma}$ on the transformation surface is greater than the work done by any $\boldsymbol{\sigma}^*$ on the i side of the transformation surface for the same jump in transformation strain, and the transformation work is the same for all stresses on the transformation surface. The principle of maximum transformation work is similar to the corresponding principle in plasticity theory.

Alternatively, starting with Eq. (46), one can prove (45) and nonconcavity of the region of metastability of each phase. All results of this subsection are valid for stability regions of phases as well.

If jumps in thermal strain and elastic compliance are taken into account, then the left-hand side of Eq. (45) is generalized to $\boldsymbol{\varepsilon}_{tj} - \boldsymbol{\varepsilon}_{ti} + \boldsymbol{\varepsilon}_{\theta j} - \boldsymbol{\varepsilon}_{\theta i} + \boldsymbol{\sigma} : (\boldsymbol{\lambda}_j - \boldsymbol{\lambda}_i)$. The transformation and phase equilibrium surfaces are not planar if $\boldsymbol{\lambda}_j - \boldsymbol{\lambda}_i \neq 0$. The associated transformation rule and the noncon-

cavity of transformation surfaces at the macroscopic level (after averaging over the representative volume) were derived in Refs. 13,14.

VI. EQUILIBRIUM AND TRANSFORMATION CONDITIONS FOR THE NiAl CUBIC-TETRAGONAL PT

NiAl austenite has cubic symmetry (CsCl structure). The crystal lattice of the martensite has been determined by transmission electron microscopy to be face-centered tetragonal (CuAu I structure).[15] We now use the results of molecular dynamics (MD) simulations[16,17] to determine

the values of ε_0, ΔG^θ, a, $\bar{A}$, θ_e, A_0, and θ_c for the NiAl cubic-tetragonal PT.

The internal energy density Φ of NiAl at zero temperature has been calculated as a function of strain by means of classical MD based on an embedded-atom method (EAM) interatomic potential.[16] At $\theta=0$, i.e., zero kinetic energy in the initial configuration, the MD algorithm simply relaxes the system into a minimum energy state for a given strain tensor. The results in Ref. 16 were presented in the form of a polynomial approximation to Φ. Since the cubic-tetragonal PT is completely described by the three principal components ε_i $(i=1,2,3)$ of the strain tensor, we can neglect terms in Φ that involve shear strains with the result

$$\Phi = 1.0875(\varepsilon_1^2+\varepsilon_2^2+\varepsilon_3^2)+1.616(\varepsilon_1\varepsilon_2+\varepsilon_1\varepsilon_3+\varepsilon_2\varepsilon_3)-6.687(\varepsilon_1^3+\varepsilon_2^3+\varepsilon_3^3)-6.117\varepsilon_1\varepsilon_2\varepsilon_3$$
$$-3.112(\varepsilon_1^2\varepsilon_2+\varepsilon_1\varepsilon_2^2+\varepsilon_1^2\varepsilon_3+\varepsilon_2^2\varepsilon_3+\varepsilon_1\varepsilon_3^2+\varepsilon_2\varepsilon_3^2)$$
$$+490.8(\varepsilon_1^2\varepsilon_2\varepsilon_3+\varepsilon_1\varepsilon_2^2\varepsilon_3+\varepsilon_1\varepsilon_2\varepsilon_3^2)+250.25(\varepsilon_1^2\varepsilon_2^2+\varepsilon_1^2\varepsilon_3^2+\varepsilon_2^2\varepsilon_3^2)$$
$$+171.83(\varepsilon_1^3\varepsilon_2+\varepsilon_1\varepsilon_2^3+\varepsilon_1^3\varepsilon_3+\varepsilon_2^3\varepsilon_3+\varepsilon_1\varepsilon_3^3+\varepsilon_2\varepsilon_3^3)+58.54(\varepsilon_1^4+\varepsilon_2^4+\varepsilon_3^4). \tag{47}$$

The coefficients in Eq. (47), which are in units of 10^5 MPa, were found by a least-squares fit to the calculated energy with a greater weighting given to points near the A and M_i minima as well as along the minimum-energy paths between the minima (weighting factors were not provided in Ref. 16). At the minimum of the internal energy density (47), the transformation strain and corresponding value $\Phi_{\min}$ are given by

$$\boldsymbol{\varepsilon}_{t1}=\{0.215;-0.078;-0.078\},$$
$$\Delta G^\theta(0)=\Phi_{\min}=-315.6 \text{ MPa}; \tag{48}$$

the tensors $\boldsymbol{\varepsilon}_{t2}$ and $\boldsymbol{\varepsilon}_{t3}$ can be obtained by permutation of components. The zero-temperature elastic moduli $C_{ij}=\partial^2\Phi/\partial\varepsilon_i\partial\varepsilon_j$ at $\boldsymbol{\varepsilon}=0$ (A) and $\boldsymbol{\varepsilon}=\boldsymbol{\varepsilon}_{t1}$ (M) are

$$C_{11}^A=C_{22}^A=C_{33}^A=2.175, \quad C_{12}^A=C_{13}^A=C_{23}^A=1.616,$$
$$C_{11}^M=4.538, \ C_{22}^M=C_{33}^M=7.449, \ C_{12}^M=C_{13}^M=3.967,$$
$$C_{23}^M=3.445. \tag{49}$$

Comparison of the zero-temperature elastic moduli of A to room-temperature experimental data[18] shows discrepancies of 8% for C_{11}^A, 15% for C_{12}^A, and 11% for $C'=(C_{11}^A-C_{12}^A)/2$, but the discrepancy was 32% for C_{44}^A. However, since the PT is controlled primarily by C', the discrepancy in C_{44} is inconsequential for the cubic-tetragonal PT.[18] Experimental values for the third-order elastic constants and the elastic constants of M are not available in the literature. We expect that our Landau model parameters determined from Eq. (47) are generally accurate to 20% or better.

We estimate that at the highest PT stress the jumps in the components of elastic strain do not exceed 4% of the corre-

sponding transformation strain components, hence we neglect terms in the PT criteria that involve jumps in elastic compliance; the resulting error does not exceed 2%. Throughout the remainder of this section, stresses and energy densities are in units of MPa and temperatures are in degrees K where units are not explicitly indicated.

The parameters A and a are determined by first finding the stress tensors for the direct and reverse PT and then substituting them in the $A\leftrightarrow M$ PT criteria (4). For $\varepsilon_2=\varepsilon_3$ the level curves of Φ are nearly parallel to $\boldsymbol{\varepsilon}_{t1}$. Consequently, the minimum energy path between A and M_1 is approximately $\boldsymbol{\varepsilon}=y\boldsymbol{\varepsilon}_{t1}$, where y is the transformation coordinate. Along this path the free energy is given by $\Phi=1918y^2-5096y^3+2862y^4$. PT occur at the two y values satisfying the stability condition $d^2\Phi/dy^2=0$, namely, $y=0.1511$ ($A\rightarrow M_1$) and $y=0.7391$ ($M_1\rightarrow A$). Substitution of the strains corresponding to these y values into the expression for the stress tensor $\sigma_i=\partial F/\partial\varepsilon_i$ yields the PT stresses: $\boldsymbol{\sigma}=\{1664, 565.2, 565.2\}$ for $A\rightarrow M_1$ and $\boldsymbol{\sigma}=\{-4054, 140.6, 140.6\}$ for $M_1\rightarrow A$. Inserting these stresses into the PT criteria (4) one obtains $A=805.2$ and $a=2.980$.

The barrier parameter $\bar{A}$ can be determined from the $M_2\rightarrow M_1$ PT criterion (6). We investigated the Gibbs potential $G=\Phi-\boldsymbol{\sigma}{:}\boldsymbol{\varepsilon}$ for the twinning transformation $M_2\leftrightarrow M_1$ as a function of the shear stress $\boldsymbol{\sigma}=\{\sigma,-\sigma,0\}$ in the twinning direction. The minimum of G corresponding to M_2 disappears at $\sigma=3026$. Substituting this value into Eq. (6) we find $\bar{A}=5320$.

It is interesting to note that after the disappearance of the M_2 minimum, the system falls into a new minimum at $\boldsymbol{\varepsilon}=\{0.02753, -0.03353, 0.003995\}$ which corresponds to a metastable orthorhombic phase. This phase is an artifact of the complex polynomial (47), which may have other non-

physical minima. This minimum disappears at $\sigma = 3170$. Our potential has no unphysical minima for D sufficiently small.

In principle, the parameters D and B can be determined by fitting our potential to MD data at points away from both the A and M_i minima and the minimum-energy paths between the minima. However, Φ was not calculated at such points so B and D cannot be reliably determined from Eq. (47). Consequently, we assume $B = 0$ and bound the constant D by requiring that $G(\sigma,0,1,1) \geqslant G(\sigma,0,1,0)$ is satisfied under uniaxial compressive loading, which imposes more restrictive bounds on D than tensile loading, and that nonphysical minima are absent from the Gibbs potential. At $\sigma = -7000$, which is far outside the region of stability of M_1 and consequently far beyond stresses of interest, the condition $G(\sigma,0,1,1) = G(\sigma,0,1,0)$ is fulfilled at $D = 1438$, but there is a nonphysical local minimum along the line $\eta_1 = 1$. This minimum disappears at $D = 500$, so we choose this value, which ensures that no unphysical minima occur at smaller compressive stresses or in tension.

The critical temperatures depend on the value of the equilibrium temperature θ_e. EAM MD calculations of θ_e for NiAl show a strong dependence on Ni content.[17] Of the three compositions for which θ_e was calculated in Ref. 17, the volumetric strain, $\varepsilon_0 = \varepsilon_{ti}^{11} + \varepsilon_{ti}^{22} + \varepsilon_{ti}^{33}$, of $Ni_{61}Al_{39}$, namely, 0.04, is the closest to 0.059, the value of ε_0 obtained from Eq. (48). The cubic-tetragonal equilibrium temperature of the $Ni_{61}Al_{39}$ was calculated to be 215 K. If we take Eq. (29), it then follows from Eq. (48) and the values of A and a at $\theta = 0$ K that $A_0 = 4.40$ and $\theta_c = -183$ K, and that the temperature of M loss of stability is $\bar{\theta}_c = 2\theta_e - \theta_c = 613$ K.

Substituting $\varepsilon_0 = 0.059$, $a = 2.98$, $\bar{A} = 5320$ MPa, $B = 0$, $D = 500$ MPa, $\theta_e = 215$ K, $A_0 = 4.40$ MPa K^{-1}, and $\theta_c = -183$K in Eqs. (38) and (43) gives the phase equilibrium and transformation conditions for NiAl ($i \neq k \neq l$):

$$A - M_i: \quad 0.215S_i - 0.078(S_k + S_l) = -316 + 1.47\theta - 0.059\sigma_0,$$

$$M_l - M_k: \quad S_l = S_k,$$

$$A \rightarrow M_i: \quad 0.215S_i - 0.078(S_k + S_l) \geqslant 270 + 1.48\theta - 0.059\sigma_0,$$

$$\hspace{10cm}(50)$$

$$M_i \rightarrow A: \quad 0.215S_i - 0.078(S_k + S_l) \leqslant -894 + 1.46\theta - 0.059\sigma_0,$$

$$M_l \rightarrow M_k: \quad (S_k - S_l) \geqslant 6050.$$

For uniaxial loading in the [001] direction, Eq. (22) of part I gives

$$\sigma = \frac{1260 + 6.87\theta - 5470\eta}{1 + 0.0134\eta}. \hspace{2cm} (51)$$

The $A \rightarrow M$ PT occurs at $\sigma = 1260 + 6.87\theta$, and the reverse PT takes place at $\sigma = -4150 + 6.78\theta$; the stress hysteresis $5410 + 0.09\theta$ is practically temperature independent. The maximal known experimental value of the temperature derivative of the transformation stress is 3.03.[19] This is smaller than the value predicted by our Landau model, namely, 6.84, because of crystal defects.

The NiAl phase equilibrium and transformation conditions can be analyzed geometrically using the diagrams presented in Sec. V. The phase equilibrium diagram is Fig. 4(a) with the distance between the center and the side of the triangle equal to $6.16(\theta - 215) - 0.087\sigma \geqslant 0$, or Fig. 5 if the inequality is reversed. Fig. 7 is the phase transformation diagram for the pseudoelastic regime $(-894 + 1.46\theta - 0.059\sigma_0 > 0)$. The stress hysteresis in the deviatoric plane for the $A \leftrightarrow M_i$ PT is $h_{AM} = 3445 + 0.059\theta$, and that for variant-variant transformations is $h_{MM} = 2\sqrt{2}\bar{A}/(9\varepsilon) = 8560$. Figure 7(a) is the phase transformation diagram if $h_{MM} > \tan(\pi/6)h_{AM}$, which is the case for $\theta < 1.9 \times 10^5 K$. Consequently, the "double" PT $M_i \rightarrow A \rightarrow M_j$ may occur at any temperature. Figure 8 corresponds to the condition $-894 + 1.46\theta - 0.059\sigma_0 = 0$.

VII. CONCLUDING REMARKS

We have constructed a three-dimensional Landau theory for multivariant stress-induced martensitic phase transformations. The material parameters characterizing both stable and unstable states can be obtained from a combination of experiment and molecular dynamics simulations. In contrast to previous models, ours can incorporate all temperature-dependent thermomechanical properties of both phases, including higher-order elastic properties; describes transformations between austenite and martensitic variants and between martensitic variants for any type of symmetry of A and M; and describes typical stress-strain curves with constant transformation-strain tensors (temperature and stress independent), constant or weakly temperature dependent stress hysteresis, and transformation at nonzero tangent moduli, in agreement with experimental stress-strain relations.

Geometric representations of the conditions for phase equilibrium and phase transformations in six-dimensional stress space were developed. The utility of these representations was exemplified by the cubic-tetragonal PT for which equilibrium and transformation surfaces in three-dimensional stress space and the corresponding lines in the deviatoric-stress plane were determined at various temperatures, and transformation processes were analyzed. The free energy (hyper) surface topography can lead to nontrivial transformation processes, e.g., variant-variant transformation through virtual A, or $M_i \rightarrow A$ PT along a path that includes deformation in the direction of $M_j (j \neq i)$. An associated transformation rule, similar to that for plasticity, was found. And finally, the phase equilibrium and transformation conditions for the NiAl cubic-tetragonal PT were determined.

The qualitative differences in the characteristics of direct and reverse PT, stress hysteresis, and variant-variant transformations between our model and previous models will lead to substantial differences in the predicted structure of interfaces and the sensitivity to crystal defects. We expect that the effect of stress concentration around defects, which is proportional to the elastic moduli, will be more pronounced in our theory than, for example, in Ref. 11, because tangent elastic moduli do not tend to zero in our Landau model.

The quantitative study of a number of important problems concerning temperature- and stress-induced martensitic PT

can be carried out using our three-dimensional Gibbs free energy. Problems of interest include the following.

- Heterogeneous martensite nucleation. It is known that the thermodynamic driving force to cause PT in defect-free Fe-Co precipitates in a copper matrix is seven times larger than in the same precipitates containing dislocations.[20] Our Landau model can be used as the basis for quantitative studies of the appearance of martensitic embryos and nuclei at dislocation aggregates such as dislocation pile ups, and tilt and grain boundaries. Research to date[10,11,21] has been based on Landau models, discussed in the Introduction to part I, with significant shortcomings.

- Martensite nucleation at crack tips. Stress concentration near crack tips may induce martensitic PT. An increase in the fracture toughness because of PT is an important strengthening mechanism called transformation toughening.[10,16] The quantitative prediction of the effect of PT on fracture is of considerable practical importance.

- Formation and evolution of twinned microstructure.[4–6,8] The barrier height for variant-variant transformations is a key parameter that controls twinning and the mobility of variant-variant and A-M interfaces. In contrast to previous Landau models, we introduced this parameter explicitly and can study its effect on twinning and interface mobility in real materials.

- Defect generation during PT and the interaction between PT and plasticity. High internal stresses due to transformation strain usually lead to dislocation generation and a reduction in elastic energy through the formation of invariant plane strain variants. An interface with dislocations (semi-coherent interface) has a different mobility than a coherent interface. The mobility of the interface is determined primarily by the interaction of the interface with existing dislocations and dislocations generated during plastic deformation. Moreover, strain-induced nucleation takes place at defects produced during plastic flow. The interplay between PT and plasticity is one of the most complex but important problems in PT theory.

- Transition from slip to twinning as an accommodation mechanism during martensite nucleation and growth. The transition is strongly temperature dependent and may even occur within a single martensite plate. This transition is expected to be very sensitive to the form of the Landau potential for variant-variant transformations.

- Structure of interfaces, solitary waves, and the interaction of moving interfaces with defects.[21–25] The majority of work on this topic has been based on polynomials in the strain. Interface structure has been investigated primarily for the stress-free case. Studies utilizing our more physically realistic Landau model for non-zero stress may lead to new results. If it is found that the interface energy varies significantly with stress then that dependence should be accounted for in mesoscale models of stress-induced nucleation and growth.

The description of martensitic PT in steels, carbon and boron nitrides, and the majority of high pressure PT would necessitate the generalization of our Landau model to the geometrically nonlinear case, i.e. large elastic and transformational strains, and material rotation. Some aspects of the kinematic and thermodynamic formalism developed in Ref. 26 outside the context of Landau theory can be of help in generalizing our model.

Stress hysteresis is constant or weakly temperature dependent in our model. At the same time, experimental stress-strain curves exhibit much greater stress hysteresis at θ_e, i.e., in the pseudoplastic regime, than in the pseudoelastic regime. Even if the barrier for the variant-variant transformation is significantly increased, the stress-strain curve is not affected because variant-variant transformation will occur via virtual A with a $M_i \to A$ PT barrier. Our Landau model does not properly describe the experimental, macroscopic stress-transformation-strain behavior because the data relate the transformation strain to the applied (macroscopic) stress while the model relates the strain to the local (microscopic) stress, which is a superposition of the applied stress and internal stresses arising from the microstructure. Thus, the description of the macroscopic stress-transformation-strain behavior requires that the internal stresses due to fine multivariant microstructure, interface surface energy (which may suppress transformation through virtual A), and defect resistance to martensite-martensite interface motion be taken into account. This can be achieved by means of large-scale numerical simulations based on a microscopic Landau model such as ours. This numerical coarse-graining approach is occasionally circumvented by applying Landau theory directly on a macroscopic scale; see, for example, Ref. 27. There is an implicit assumption that the effect of defects is approximately included in the parameters of the potential as is done, for example, in macroscopic plasticity theory. Our Landau model is particularly well suited for use on a macroscopic scale because its stress-strain curves possess all of the basic features of macroscopic stress-strain curves in the pseudoelastic regime. Moreover, it does not suffer from the shortcomings of the Landau potential proposed in Ref. 27 for zirconia ceramics, namely an incorrect sign for an elastic modulus and unequal transformation strains for direct and reverse PT.

ACKNOWLEDGMENTS

*Email address: valery.levitas@coe.ttu.edu

[1] V.I. Levitas and D.L. Preston, preceding paper, Phys. Rev. B **66**, 134206 (2002).

[2] E.K.H. Salje, *Phase Transitions in Ferroelastic and Co-Elastic Crystals* (Cambridge University Press, New York, 1990).

[3] T. Ichitsubo, K. Tanaka, M. Koiwa, and Yo. Yamazaki, Phys. Rev. B **62**, 5435 (2000).

[4] A. Saxena, Y. Wu, T. Lookman, S.R. Shenoy, and A.R. Bishop, Physica A **239**, 18 (1997).

[5] S.R. Shenoy, T. Lookman, A. Saxena, and A.R. Bishop, Phys. Rev. B **60**, R12 537 (1999).

[6] Y. Wang and A.G. Khachaturyan, Acta Mater. **45**, 759 (1997).

[7] Y.H. Wen, Y. Wang, and L.Q. Chen, Acta Mater. **47**, 4375 (1999).

[8] A. Artemev, Y. Wang, and A.G. Khachaturyan, Acta Mater. **48**, 2503 (2000).

[9] A. Artemev, Y. Jin, and A.G. Khachaturyan, Acta Mater. **49**, 1165 (2001).

[10] A.A. Boulbitch and P. Toledano, Phys. Rev. Lett. **81**, 838 (1998).

[11] A.C.E. Reid, G.B. Olson, and B. Moran, Phase Transitions **69**, 309 (1998).

[12] J. Lubliner, *Plasticity Theory* (Macmillan, New York, 1990).

[13] V.I. Levitas, in *Proceedings Of Fourth International Conference On Constitutive Laws For Engineering Materials: Experiment, Theory, Computation and Applications*, edited by R.C. Picu and E. Krempl (RPI, Troy, NY, 1999), pp. 309–312.

[14] V.I. Levitas, A.V. Idesman, and E. Stein, J. Intell. Mater. Syst. Structure **10**, 983 (1999).

[15] K. Enami, S. Nenno, and K. Shimizu, Trans. Jpn. Inst. Met. **14**, 161 (1973).

[16] P.C. Clapp, C.S. Besquart, Y. Shao, Y. Zhao, and J.A. Rifkin, Modell. Simul. Mater. Sci. Eng. **2**, 551 (1994).

[17] S. Rubini and P. Ballone, Phys. Rev. B **48**, 99 (1993).

[18] Y. Shao, P.C. Clapp, and J.A. Rifkin, Metall. Mater. Trans. A **27**, 1477 (1994).

[19] T. Davenport, C. Grehofsky, M. Gonzalez, J. Worgull, and J. Trivisonno, J. Phys. IV **5**, 1023 (1995).

[20] M. Lin, G.B. Olson, and M. Cohen, Acta Metall. Mater. **41**, 253 (1993).

[21] W. Cao and J.A. Krumhansl, Phys. Rev. B **42**, 4334 (1990).

[22] G.R. Barsch and J.A. Krumhansl, Phys. Rev. Lett. **53**, 1069 (1989).

[23] F. Falk, Z. Phys. B: Condens. Matter **51**, 177 (1983).

[24] A.E. Jacobs, Phys. Rev. B **46**, 8080 (1992).

[25] L. Truskinovsky, Continuum Mech. Thermodyn. **6**, 185 (1994).

[26] V.I. Levitas, Int. J. Solids Struct. **35**, 889 (1998).

[27] B. Budiansky and L. Truskinovsky, J. Mech. Phys. Solids **41**, 1445 (1993).